optica

Efficient terahertz and Brunel harmonic generation from air plasma via mid-infrared coherent control: supplementary material

DOGEUN JANG, ROBERT M. SCHWARTZ, DANIEL WOODBURY, JESSE GRIFF-MCMAHON, ABDURRAHMAN H. YOUNIS, HOWARD M. MILCHBERG, AND KI-YONG KIM*

Institute for Research in Electronics and Applied Physics, University of Maryland, College Park, MD 20742, USA
**Corresponding author: kykim@umd.edu*

Published 10 October 2019

This document provides supplementary information to "Efficient terahertz and Brunel harmonic generation from air plasma via mid-infrared coherent control," https://doi.org/10.1364/OPTICA.6.001338.

1. Experimental setup

In Fig. 1, a 200-μm thickness GaSe crystal (z-cut) with 12 mm diameter is placed 75 mm away from the lens for copropagating second harmonic (1.95 μm) generation. Two rotation axes (α and β) are controlled for optimal THz generation. The incidence angle ϕ of a thin (170 μm) coverslip glass is varied to control the relative phase θ between 3.9 μm and 1.95 μm pulses. An off-axis (90°) parabolic (OAP) mirror (f = 100 mm) with a hole is used to reflect and collimate THz radiation emitted from the air plasma while transmitting laser and harmonic radiation. An ITO coated window is used to separate optical and near-infrared light for spectral measurements with fiber-coupled optical (Ocean Optics, HR2000+) and near-infrared (Avantes, NIRLine) spectrometers. The emitted THz radiation is filtered by a pair of 7-μm longpass cut-off filters and detected with a pyroelectric detector (Gentec-EO Inc., QS9-THz-BL) or a microbolometer focal plane array (FLIR, Tau2). A Fourier transform infrared (FTIR) spectrometer (not shown) is used to characterize emitted THz spectrum.

2. Second harmonic generation (SHG) in GaSe

GaSe is a popular nonlinear crystal often used for SHG at the mid-infrared due to its large nonlinearity (d_{22} = 54 pm/V at 10.6 μm) and relatively high damage threshold (>3×10^{10} W/cm^2) [1]. The indices of refraction along the ordinary and extraordinary axes are n_o = 2.73 and n_e = 2.40 at 3.9 μm and n_o = 2.75 and n_e = 2.42 at 1.95 μm [2]. Those yield relatively large Fresnel losses (~17% per each surface), providing ~69% transmission but negligible absorption (α = 0.05–0.1 cm^{-1}) [1] in our 200 μm thick crystal. We observe both Type 0 (e + e → e) and Type 1 (o + o → e) SHG in our ε-GaSe. This is confirmed by measuring the polarization property of the produced 2ω with a mid-infrared polarizer (see Fig. 2(b)). The green and magenta lines in Fig. 2(b) correspond to Type 0 (parallel ω and 2ω) and Type 1 (perpendicular ω and 2ω) SHG, respectively. Here Type 0 is chosen for efficient terahertz (THz) radiation as two-color fields with parallel polarization maximally produces a directional plasma current. In Type 0 at α = 30°, the coherence length for phase matching, $\lambda_\omega/[2(n_{2\omega} - n_\omega)]$, is estimated to be 130 μm, comparable to the crystal thickness for sufficient SHG. The expected group velocity walk-off between 3.9 μm and 1.95 μm is 24 fs in our 200-μm thick GaSe. This, however, is mostly compensated by a similar but opposite group velocity walk-off occurring in the following coverslip glass.

The energy ratio of 2ω to ω is measured by two independent methods. First, a thin (<200 μm) mid-infrared polarizer (Thorlabs LPMIR100) with known transmission and extinction ratios at 1.5–5 μm is used to measure the transmitted energy (ω and 2ω) of both horizontal and vertical polarization components under Type 1 SHG at α = 60° (see Fig. 2(b)). Then the 2ω energy under Type 0 at α = 30° is determined from the relative SH yield from Fig. 2(a). This provides an energy ratio of 2%. Second, the combined energy (ω and 2ω) right after the GaSe under Type 0 is measured with an additional BK7 filter of 10 mm thickness that mostly transmit 2ω (1.95 μm) but strongly absorbs ω (3.9 μm) radiation. From known BK7 absorption and Fresnel losses at both wavelengths, the relative energy ratio is estimated to be 2.4%. As the first method is

more reliable, a relative energy ratio of 2% is selected for further analysis.

We have also observed third harmonic radiation directly produced from the GaSe crystal. However, its energy is extremely weak (0.3% of SH) and thus provides negligible contributions to the plasma current generation. GaSe can also generate THz radiation directly via optical rectification [3-5]. But no measurable THz emission was observed from our crystal. This is possibly due to our unfavorable phase matching condition for optical rectification and THz absorption/attenuation in the coverslip glass and air plasma.

3. Phase control by window tilting

A 170-μm thickness coverslip glass (Thorlabs CG15KH1) is used to control the initial relative phase θ_0 between ω (ω_1) and 2ω (ω_2) pulses (see Fig. S1(a)). Here the angle of refraction is given by $\phi_1 = \sin^{-1}(\sin\phi/n_1)$ and $\phi_2 = \sin^{-1}(\sin\phi/n_2)$ from Snell's law, where $n_{1,2}$ is the refractive index of the coverslip at the fundamental (ω_1) and second harmonic (ω_2) frequency, respectively, and ϕ is the incidence angle. Then the relative phase shift obtained from material dispersion at ϕ is given by $\theta_0(\phi) = 2\pi t\{n_2(\lambda_2\cos\phi_2)^{-1} + \sin\phi\,(\tan\phi_1 - \tan\phi_2)\lambda_2^{-1} - 2n_1(\lambda_1\cos\phi_1)^{-1}\}$, where t is the thickness of the coverslip and $\lambda_{1,2}$ is the wavelength at ω_1 and ω_2, respectively. The above relationship, $\theta_0 = \theta_0(\phi)$, is used to convert THz yields measured as a function of ϕ (see Fig. S1(b)) to corresponding θ_0-dependent THz outputs as shown in Fig. 3(f). We note that the coverslip results in a laser energy loss of ~10%. The expected temporal walk-off between the ω and 2ω pulses is ~20 fs at ϕ = 42° where maximal THz radiation is produced. The transverse beam walk-off is negligible (~1 μm) compared to the focused beam size (~60 μm in HWHM).

Alternatively, air dispersion is used instead of the coverslip glass to control the initial relative phase θ_0. In this case, the collimated fundamental (ω) pulse is frequency doubled in GaSe without focusing (no CaF_2 lens used). Then the two-color laser pulses are focused by an off-axis (90°) parabolic (OAP) mirror for THz generation. Here the separation between the GaSe crystal and OAP mirror is adjusted to control θ_0. In this configuration, we measure the dephasing length [6] of ~0.90 m in air, over which the local THz polarity remains the same ($0 \le \theta_0 \le \pi$ between 3.9 μm and 1.95 μm). We find that this method, however, is not suitable for a phase control because of undesirable beam mode changes with propagation in our experiment.

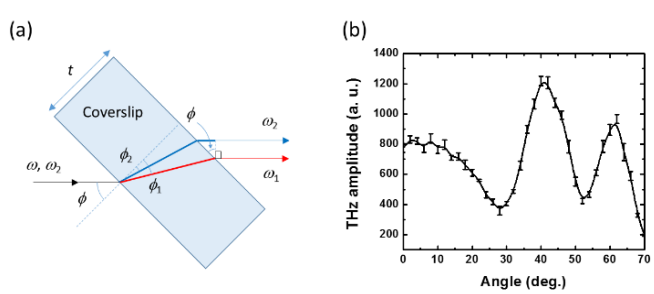

Fig. S1. (a) Relative phase θ_0 control between ω_1 (ω) and ω_2 (2ω) pulses by rotation of a thin coverslip glass. (b) THz output yield as a function of the coverslip rotation angle ϕ.

4. THz and harmonic measurements and calibrations

THz energy is measured with a lithium tantalite ($LiTaO_3$) pyroelectric detector that has a sensing diameter of 9 mm (Gentec-EO Inc., QS9-THz-BL). This pyroelectric sensor has an organic black coating, which has a relatively flat response curve over a broad range of optical and infrared frequencies (7.5 – 3000 THz). At below ~7.5 THz, the detector's sensitivity gradually drops with decreasing frequency, reaching about ~10% of its flat value at 1 THz. Because of this, the THz energy we measure is underestimated when THz radiation below 7.5 THz is included. The pyroelectric detector is calibrated at near-infrared and mid-infrared wavelengths (0.8 μm and 3.9 μm), which both provides a similar responsivity of 260 kV/W at a repetition rate of 20 Hz (or 0.19 μJ/V per pulse at 20 Hz). The spectral transmission of the two 7-μm longpass filters, used to cut-off radiation at >40 THz, is determined from combined FTIR measurements with commercial (Shimadzu, IR Prestige21) and lab-built spectrometers operating at >12 THz and <12 THz frequency ranges, respectively. This is used to correct the THz radiation spectrum shown in Fig. 4(a).

We note that the maximum laser-to-THz conversion efficiency of 1% ± 0.2% is obtained with 3 filters (two longpass and one Si filters) placed in the THz beam path. Here we calibrated THz transmission for each filter, longpass (17% each) and Si (33%), using the emitted THz radiation.

The variation of THz local emission energy along the laser propagation direction, z, is determined by an aperture scanning method [6]. An iris with an aperture radius of $a = 2$ mm is used to block the THz waves emitted in front the iris, while the THz waves generated behind the iris are unblocked and detected. Basically, it measures $S(z_a) = \int_z^\infty |E_{\mathrm{THz}}(z)|^2\,dz$, where $z_a = z + a/\tan\Theta$ is the position of the aperture and $\Theta = 2.4°$ is the half divergence angle of THz radiation, obtained from Fig. 1(c). The derivative of the signal, $-dS(z_a)/dz$, represents the variation of local THz intensity $|E_{\mathrm{THz}}(z)|^2$ along z as shown in Fig. 3(c).

The spectral responses of the fiber-coupled optical (for 2nd – 3rd harmonics) and near-infrared (4th – 9th) spectrometers are calibrated with a quartz tungsten halogen (QTH) lamp. The 3rd harmonic (1.3 μm) is detected by both spectrometers and used as a reference to fuse two spectral measurements as shown in Fig. 5(a). The spectral power of the SH relative to the fundamental at 3.9 μm is determined by the measured energy ratio 2%. Finally, the THz spectral power is determined from its measured conversion efficiency 1% with respect to the fundamental.

5. THz and harmonic generation simulation

Simulations of two-color laser mixing used the two-dimensional (r, z) unidirectional pulse propagation equation model (UPPE) [7]. The carrier-resolved UPPE model independently evolves each frequency component, allowing for multi-color fields and harmonic generation. We included a model for tunnel ionization of O_2, N_2, and Ar, third order susceptibility of air (with no rotation) [8, 9], and the contribution from the plasma current density [10].

To match experimental conditions, we generated 120 fs Gaussian pulses with 2.1 mJ in the fundamental and 10.5 μJ in the second harmonic focused to peak intensities >10^{14} W/cm^2. An arbitrary offset was added at the input to control the relative phase between the fundamental and second harmonic.

Our simulation window covers 3000 fs with 2^{15} points which covers a frequency space from 0.33 THz to 11 PHz. This yields a temporal step size of 0.09 fs, about 70 times smaller than the period of the second harmonic pulse at 1.95 μm. High frequencies >1.5 PHz (200 nm) are strongly attenuated—corresponding to

strong UV absorption in air. Spatially we resolve a 4 mm radius space with 400 points for a step size of 10 μm. The whole simulation is solved over 15 cm of propagation with the vacuum focus at z = 10 cm and a beam waist of ~100 μm, resulting in peak laser intensities of 110-130 TW/cm^2 and electron densities of 4-5 $\times 10^{16}$/cm^{-3} (see Fig. S2). The resulting radiation is integrated over space at z = 15 cm to find the total output spectrum.

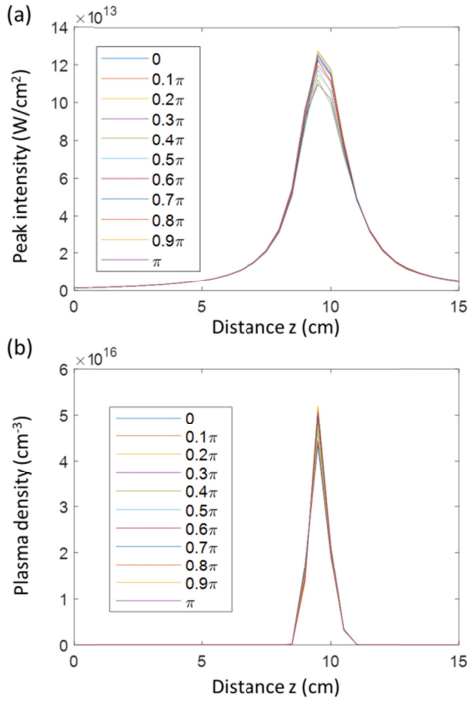

Fig. S2. (a) On-axis peak laser intensity and (b) electron density as a function of propagation distance z with various initial relative phases assigned at z = 0. The vacuum focus is located at z = 10 cm.

We also present a simple semi-classical calculation of refractive index transients induced by plasma versus $\chi^{(3)}$ effects as shown in Fig. S3. It shows that the plasma effect is dominant at a single atom level under our experimental condition (3.9 μm, 130 TW/cm^2). Here the amount of refractive index transients is considered to be a simple measure of nonlinear contributions in producing new frequency radiation including low-order harmonics.

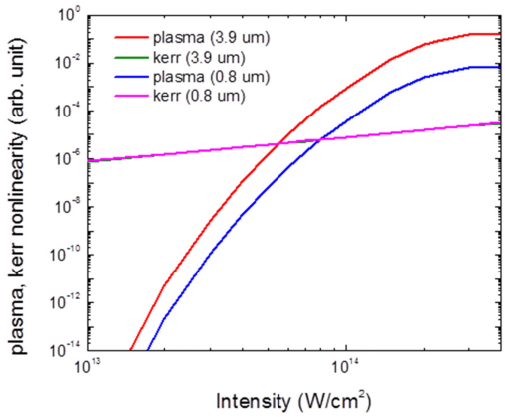

Fig. S3. Relative refractive index transients due to plasma generation (red and blue lines) and $\chi^{(3)}$ from bound electrons (green and magenta lines) as a function of laser intensity at the wavelength of 0.8 μm and 3.9 μm. Here $\chi^{(3)} = 7.9 \times 10^{-20}$ cm^2/W [9] is used for both 0.8 μm and 3.9 μm. Here a tunneling ionization model for nitrogen is used [8,9,11].

References

1. V. G. Dmitriev, G. G. Gurzadyan, and D. N. Nikogosyan, Handbook of Nonlinear Optical Crystals (Springer, Berlin, 1999).
2. K. Kato, F. Tanno, and N. Umemura, "Sellmeier and thermo-optic dispersion formulas for GaSe (Revisited)," Appl. Opt. **52**, 2325 (2013).
3. R. Huber, A. Brodschelm, F. Tauser, and A. Leitenstorfer, "Generation and field-resolved detection of femtosecond electromagnetic pulses tunable up to 41 THz," Appl. Phys. Lett. **76**, 3191 (2000).
4. K. Reimann, R. P. Smith, A. M. Weiner, T. Elsaesser, and M. Woerner, "Direct field-resolved detection of terahertz transients with amplitudes of megavolts per centimeter," Opt. Lett. **28**, 471 (2003).
5. K. Liu, J. Cu, and X.-C. Zhang, "GaSe crystals for broadband terahertz wave detection," Appl. Phys. Lett. **85**, 863 (2004).
6. Y. S. You, T. I. Oh, and K. Y. Kim, "Off-axis phase-matched terahertz emission from two-color laser-induced plasma filaments," Phys. Rev. Lett. **109**, 183902 (2012).
7. M. Kolesik, and J. V. Moloney, "Nonlinear optical pulse propagation simulation: From Maxwell's to unidirectional equations," Phys. Rev. E **70**, 036604 (2004).
8. S. Zahedpour, J. K. Wahlstrand, and H. M. Milchberg, "Measurement of the nonlinear refractive index of air constituents at mid-infrared wavelengths," Opt. Lett. **40**, 5794 (2015).
9. S. Zahedpour, S. W. Hancock, and H. M. Milchberg, "Ultrashort infrared 2.5-11 μm pulses: spatiotemporal profiles and absolute nonlinear response of air constituents," Opt. Lett. **44**, 4 (2019).
10. F. J. Brunel, "Harmonic generation due to plasma effects in a gas undergoing multiphoton ionization in the high-intensity limit," Opt. Soc. Am. B **7**, 521 (1990).
11. K. Y. Kim, J. H. Glownia, A. J. Taylor, and G. Rodriguez, "Terahertz emission from ultrafast ionizing air in symmetry-broken laser fields," Opt. Express **15**, 4577 (2007).